AGU PUBLICATIONS

JGR

Journal of Geophysical Research: Oceans

RESEARCH ARTICLE

10.1002/2014JC010283

Key Points:

- The air-sea drag during typhoon landfall is investigated for winds up to 40 m/s
- The drag curve shifts 15 m/s for low typhoon winds relative to the open ocean
- A water-depth-dependency C_D scheme is proposed and tested

Correspondence to:
C.X. Liu,
cxliu@grmc.gov.cn

Citation:
Zhao, Z.-K., C.-X. Liu, Q. Li, G.-F. Dai, Q.-T. Song, and W.-H. Lv (2015), Typhoon air-sea drag coefficient in coastal regions, *J. Geophys. Res. Oceans*, *120*, 716–727, doi:10.1002/2014JC010283.

Received 9 JUL 2014
Accepted 1 JAN 2015
Accepted article online 7 JAN 2015
Published online 9 FEB 2015

Typhoon air-sea drag coefficient in coastal regions

Zhong-Kuo Zhao[1,2], Chun-Xia Liu[1], Qi Li[3], Guang-Feng Dai[1], Qing-Tao Song[4,5], and Wei-Hua Lv[6]

[1]Institute of Tropical and Marine Meteorology/Guangdong Provincial Key Laboratory of Regional Numerical Weather Prediction, China Meteorology Administration, Guangzhou, China, [2]State Key Laboratory of Severe Weather, Chinese Academy of Meteorological Sciences, Beijing, China, [3]Department of Civil and Environmental Engineering, Princeton University, Princeton, New Jersey, USA, [4]National Satellite Ocean Application Service, Beijing, China, [5]Key Laboratory of Space Ocean Remote Sensing and Application, State Oceanic Administration, Beijing, China, [6]Maoming Meteorological Bureau, China Meteorology Administration, Maoming, China

Abstract The air-sea drag during typhoon landfalls is investigated for a 10 m wind speed as high as $U_{10} \approx 42$ m s^{-1}, based on multilevel wind measurements from a coastal tower located in the South China Sea. The drag coefficient (C_D) plotted against the typhoon wind speed is similar to that of open ocean conditions; however, the C_D curve shifts toward a regime of lower winds, and C_D increases by a factor of approximately 0.5 relative to the open ocean. Our results indicate that the critical wind speed at which C_D peaks is approximately 24 m s^{-1}, which is 5–15 m s^{-1} lower than that from deep water. Shoaling effects are invoked to explain the findings. Based on our results, the proposed C_D formulation, which depends on both water depth and wind speed, is applied to a typhoon forecast model. The forecasts of typhoon track and surface wind speed are improved. Therefore, a water-depth-dependence formulation of C_D may be particularly pertinent for parameterizing air-sea momentum exchanges over shallow water.

1. Introduction

Air-sea momentum exchange can be separated into frictional drag due to the molecular viscosity at the air-sea interface and the drag arising from sea-surface waves [e.g., *Donelan et al.*, 2012]. The total stress is usually parameterized in terms of the drag coefficient (C_D) or roughness length z_0. Many measurement results conclude that C_D increases approximately linearly with wind speeds from 5 to 25 m s^{-1} [e.g., *Edson et al.*, 2007; *Garratt*, 1977; *Geernaert et al.*, 1986; *Large and Pond*, 1981; *Smith et al.*, 1992; *Yelland and Taylor*, 1996]; as the wind speed continuously increases and exceeds approximately 30 m s^{-1}, the values of C_D from wind-wave tanks [*Alamaro et al.*, 2002; *Donelan et al.*, 2004; *Takagaki et al.*, 2012; *Troitskaya et al.*, 2012] and numerical wind-wave coupled models [*Liu et al.*, 2012; *Moon et al.*, 2004; *Mueller and Veron*, 2009] level off or slightly decrease. However, most field measurements [*Bell et al.*, 2012; *Holthuijsen et al.*, 2012; *Jarosz et al.*, 2007; *Powell et al.*, 2003; *Zhao et al.*, 2011] reveal significant reductions in C_D values. An exception reported by *Black et al.* [2007] showed that the values of C_D remain invariant with wind speeds above 23 m s^{-1}. Based on observational data, the critical wind speeds at which C_D peaks are 23–40 m s^{-1}, as listed in Table 1. A recent numerical simulation [*Liu et al.*, 2012] indicates that the difference in C_D values between laboratory and field results during strong winds may be due to partially developed laboratory waves, i.e., the wave ages are lower than the natural ages.

The current knowledge of C_D at extreme wind speeds has been incorporated into atmospheric and ocean-wave models [e.g., *Gopalakrishnan et al.*, 2011; *Montgomery et al.*, 2010]. Compared with the common Charnock relationship [*Charnock*, 1955], newly proposed drag parameterization schemes have improved the predictions of surface wind speeds and tracks of tropical cyclones [*Moon et al.*, 2007; *Zweers et al.*, 2010], sea-surface cooling [*Walsh et al.*, 2010; *Zedler et al.*, 2009], wave heights [*Moon et al.*, 2008], and central pressures in certain cases [*Zweers et al.*, 2010]. In the coastal wave model simulating waves nearshore (SWAN) [*Booij et al.*, 1999], the drag coefficient formulation has lower values in high winds compared with the parameterization by *Wu* [1982] and may affect the estimation of waves and storm surges [*Zijlema et al.*, 2012]. With this new C_D formulation, a lower value for the bottom friction coefficient is required to improve the agreement between model predictions and observations.

Air-sea momentum exchange is wave state dependent. Wave states in coastal areas are affected by depth-induced processes, such as shoaling, refraction, and diffraction. *Geernaert et al.* [1986] showed that the

Table 1. The Critical Wind Speed U_{10c} and the Corresponding Water Depth/Laboratory Conditions in Different Studies

	Holthuijsen et al. [2012]	*Powell et al.* [2003]	*Jarosz et al.* [2007]	This Study	*Donelan et al.* [2004]	*Troitskaya et al.* [2012]	*Alamaro et al.* [2002]
U_{10c} (m s^{-1})	40	~34	30	24	~32	25	~24
Water depth/ laboratory conditions	Open ocean	Open ocean	69–89 m	14 m	Wave tank	Wave tank	Wave tank

shallow water C_D values for wind speeds above 15 m s^{-1} are higher than those over the open ocean and attribute the difference to the variations in the surface wave energy spectrum. Based on measurements over Lake Ontario, *Anctil and Donelan* [1996] found that the wind dependence of C_D derived for shallow water differs from that of deep water. Based on an air-flow separation model, *Makin and Kudryavtsev* [2002] reproduced the increase in C_D with decreasing water depth and steepening dominant waves. *Gao et al*. [2009] investigated the differences in C_D values over open water and shallow water for wind speeds up to 20 m s^{-1}. *Toffoli et al*. [2012] suggested that C_D depends on the water depth and wave steepness. However, these studies are restricted to moderate wind speeds; the performance of C_D over shallow water at high wind speeds has not been investigated. Under the high wind speed conditions during hurricanes, the oceanic state is complicated by strong wave breaking, the production of sea spray and a less defined interface between the atmosphere and ocean [e.g., *Holthuijsen et al*., 2012; *Powell et al*., 2003]. Observations during Hurricane Bonnie [*Walsh et al*., 2002; *Wright et al*., 2001] indicate that the hurricane wave fields over the open ocean and at landfall have common features, such as wave propagation direction, but the wavelength and wave height gradually decrease as the system approaches the shore. In addition to wave breaking forced by wind, depth-induced breaking is an important mechanism of wave breaking in coastal water [*Holthuijsen*, 2007]. More observations are necessary to resolve the influence of coastal wave processes on air-sea momentum exchange in high wind regimes. Here, we investigate this problem using field measurements in typhoon conditions from a coastal site in the South China Sea. The study attempts to illustrate the impact of water depth on the behavior of C_D from low to extreme wind conditions and to explain the variation among previous studies from the perspective of a representative wave state (significant wave) in typhoon/hurricane scenarios.

The paper is organized as follows. Basic information and the measurements during the two selected typhoons are described in section 2. Section 3 presents the characteristics of wind, oceanic states, and air-sea momentum transfer over shallow water in typhoon regimes. Additionally, a new formulation of C_D is proposed as a function of both water depth and wind speed and is tested in the prediction of Typhoon Nanmadol in 2011. Comparisons with previous studies and discussions are also presented. The conclusions are summarized in section 4.

2. Measurements and Data Processing

The coastal observation tower (COT), shown in Figure 1a, was constructed in August 2008 by the Institute of Marine Meteorology of the China Meteorology Administration (ITM2/CMA). The COT is located at 21.44°N, 111.39°E, in the South China Sea and is approximately 6.5 km from the coastline (see Figure 1a), where the water depth is approximately 14 m. The COT is anchored by three huge concrete tanks on the seafloor, and the air flow modification caused by the structure is minimal; thus, no motion correction is needed. The mean and turbulent wind speeds at five levels are recorded by wind propeller anemometers (R. M. Young Company, USA) and at two levels by an eddy covariance system, as shown in the photo in Figure 1b. Since its construction, the COT has supplied reliable and continuous meteorological measurements in the air-sea surface layer, particularly in typhoon environments. The main analyzed wind data are the 1 min mean values from the multilevel wind propeller anemometers at a sampling rate of 10 Hz. To avoid reporting the wind gusts, the results from the 10 min mean wind data are also shown. The simultaneous turbulence observations from the two sonic anemometers shown in Figure 1b are inevitably contaminated in extreme typhoon conditions and are excluded from this study.

As shown in Figure 1a, two fixed buoys are deployed around the COT. A buoy with a 0.9 m diameter (Model SBF3-1, SDIOI of China) is located at 21.43°N, 111.33°E, where the water depth is 12 m. The buoy outputs

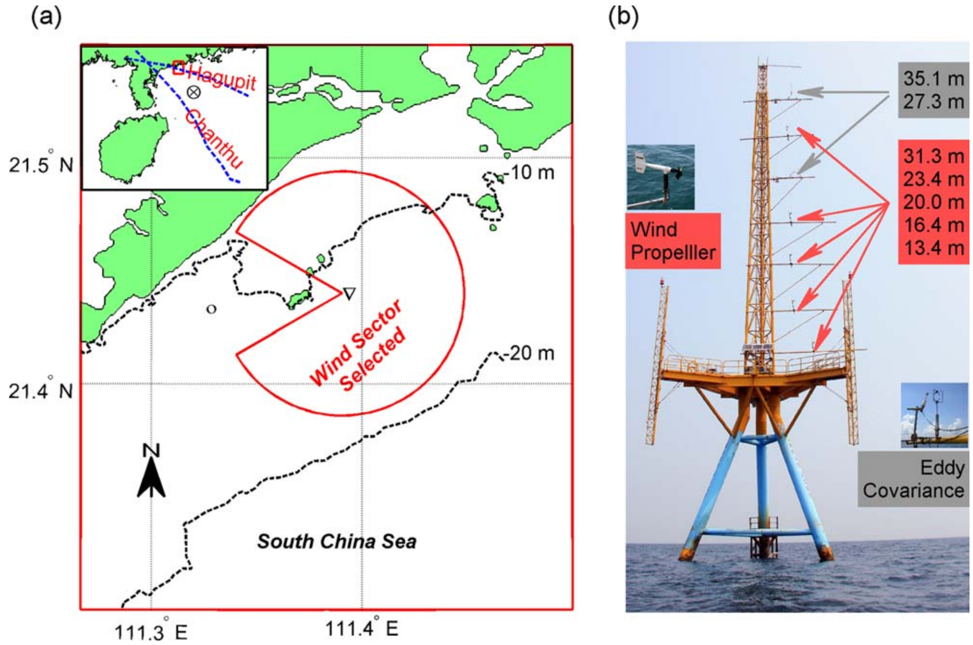

Figure 1. (a) Regional map and instrument locations. The coastal observation tower (COT) is denoted by inverted triangle. The red sector denotes the analyzed wind direction. The 0.9 m diameter buoy is denoted by bold italic circle, and the 10 m diameter buoy is denoted by crossed circle in the insert. The bathymetry (in meters) is shown for the region immediately around the tower. The blue-dashed lines in the insert denote sections of the best-path positions of Typhoon Hagupit and Chanthu according to the CMA. (b) A photo of the coastal observation tower and the instrument setup for this study. The five levels of wind propeller anemometers (R. M. Young, model: 05106), which are indicated by the red arrows, are 31.3, 23.4, 20.0, 16.4, and 13.4 m above mean sea level, and the two eddy covariance systems (gray arrows) are 35.1 and 27.3 m above mean sea level.

one group of wave parameters every 3 h, which is calculated from the first 200 waves measured in the last 22 min of each 3 h period. The 10 m diameter buoy (Model FZF4-1, SDIOI of China) is located at 20.75°N, 111.66°E, where the water depth is 60 m; this buoy outputs one group of wave parameters every 0.5 h, which is calculated from the first 200 waves sampled within the middle 20 min in each 0.5 h. The distances from the two buoys to the COT are 6.7 and 81.9 km. The wind and wave directions are specified in the nautical convention, i.e., the direction the wind or waves come from.

Based on the distance between the tropical storm center and the COT as well as the intensity of the tropical storms when approaching the COT, Typhoon Hagupit (2008) and Typhoon Chanthu (2010) are chosen for the analysis. The typhoons' tracks in relation to the COT are illustrated in Figure 1a. Basic information on the two typhoons is listed. Typhoon Hagupit was associated with a huge amount of precipitation that greatly influenced South China, and the gale-force winds triggered storm surges with a 100 year return period along the coast of Guangdong Province. A tide station [*Fu et al*., 2009] near the COT recorded a maximum water level increment of $\eta = 270$ cm. When Typhoon Hagupit made landfall on 24 September 2008, its center nearly passed over the COT. The tower recorded a minimum atmospheric pressure of 956 hPa. According to the local meteorological station at landfall, the maximum 2 min mean wind speed reached 48 m s^{-1} at a 10 m height, and the lowest pressure was 945 hPa. Typhoon Chanthu produced heavy rain that resulted in the loss of life (10 people) in mainland China. The typhoon made landfall near the city of Wuchuan, Guangdong Province, China, on 22 July 2010. According to the local meteorological station, the maximum 2 min mean wind speed at landfall was 35 m s^{-1} at a 10 m height, and the lowest pressure was 970 hPa. The distance between the best-track position and the COT was approximately 80 km. The COT recorded a maximum 10 min mean wind speed of 30 m s^{-1} at a 13.4 m height. A tide station [*Zhang et al*., 2011] near the COT recorded a storm surge of $\eta = 188$ cm.

We analyzed the data from 23 to 24 September 2008, for Typhoon Hagupit and from 21 to 22 July 2010, for Typhoon Chanthu. The profiles during the two typhoons are summarized in Figure 2 at 1 m/s intervals. For Typhoon Hagupit, the wind data are available at 16.4, 20, and 23.4 m above the mean sea surface. For Typhoon Chanthu, the wind data are available at 13.4, 16.4, 20, 23.4, and 31.3 m above the surface.

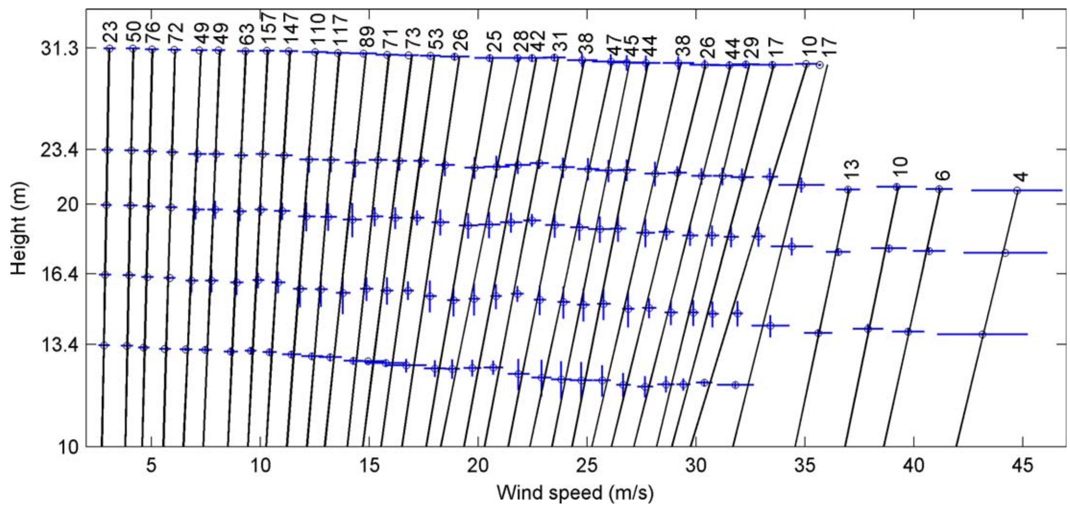

Figure 2. Mean typhoon wind profiles by sea-surface layer wind-speed group. The height is depicted as a log scale. The symbols denote the bin average of the winds and measurement heights. The horizontal bars and vertical bars in blue denote the standard deviation of the winds and the fluctuations in the measurement heights due to storm surges, respectively. The inclined lines are the lines fit by least squares using the mean in each bin. The vertical number above each line is the number of profiles in that bin. At 16.4 m, the bin width is 1 m s^{-1} for $U_{16.4} < 33$ m s^{-1} and 2 m s^{-1} for 33 m s$^{-1} \leq U_{16.4} < 39$ m s^{-1}; the winds above that speed are placed into one bin.

At high wind speeds, the atmospheric boundary layer approaches neutral stability, and the wind profile in the surface layer follows the log-law [*Stull*, 1988], as described by the following equation:

$$\frac{U_z}{u_*} = \frac{1}{\kappa} \ln\left(\frac{z}{z_0}\right), \tag{1}$$

where U_z is the Reynolds-averaged horizontal wind velocity at height z above the sea surface, $u_* = \sqrt{\tau_o/\rho}$ is the friction velocity, τ_o is the surface stress, and ρ is the air density. κ is the von-Karman constant ($\kappa=0.4$), and z_o is the roughness length. The intercept and slope of the fitted line (on a natural-log height scale) correspond to z_o and u_*/κ, respectively. This method has been used to analyze high wind profiles obtained with GPS dropsondes [*Holthuijsen et al*., 2012; *Powell et al*., 2003] as well as in numerous numerical and laboratory simulations [e.g., *Andreas*, 2004; *Mueller and Veron*, 2009]. Here, we adopt this method to select data and deduce the relevant parameters.

Because the measurement heights are at low levels (from 13.4 to 31.3 m above mean sea level), the profile method is sensitive to the water-level change in stormy conditions. To calibrate the heights of the anemometers, we use the water-level measurements from two neighboring tide stations [*Fu et al*., 2009; *Zhang et al*., 2011] during the two typhoons (Hagupit and Chanthu). Section 3 illustrates the storm surges corresponding to the selected wind data.

The data selection procedure is as follows: (1) A preparatory visual inspection is conducted according to the observer's in situ records and the physical rationality of the wind time series. (2) The wind data downwind of the tower (i.e., the data with a mean wind direction between 240° and 300°) are excluded, as shown in Figure 1a. (3) The wind profiles that do not increase with height monotonically or that have wind speeds of less than 2 m s^{-1} at the lowest level are eliminated. We measured some wind data that do not increase monotonously with height, i.e., that conflict with the log-law, and we find that these data mainly correspond to the periods when the wave speeds exceed the wind speeds and when the wind speeds are less than 2 m s^{-1}, as shown in Figure 3c. These measurements may correspond to the momentum transfer from the ocean to the atmosphere [*Grachev and Fairall*, 2001]. (4) We fit the wind profiles with equation (1) using the least squares method and reject the profiles with large fitting errors to obtain data for near-neutral conditions. Ultimately, 289 and 1441 samples of 1 min mean wind profiles for Typhoons Hagupit and Chanthu, respectively, are used in the analysis. As shown in Figure 2, the wind profiles from the two typhoons are compiled and separated into bins according to the wind data at a 16.4 m height. Notably, at least four profiles are placed in high-wind bins, and the profiles sufficiently follow the log-law. For each bin, the values of the friction velocity u_* and the roughness

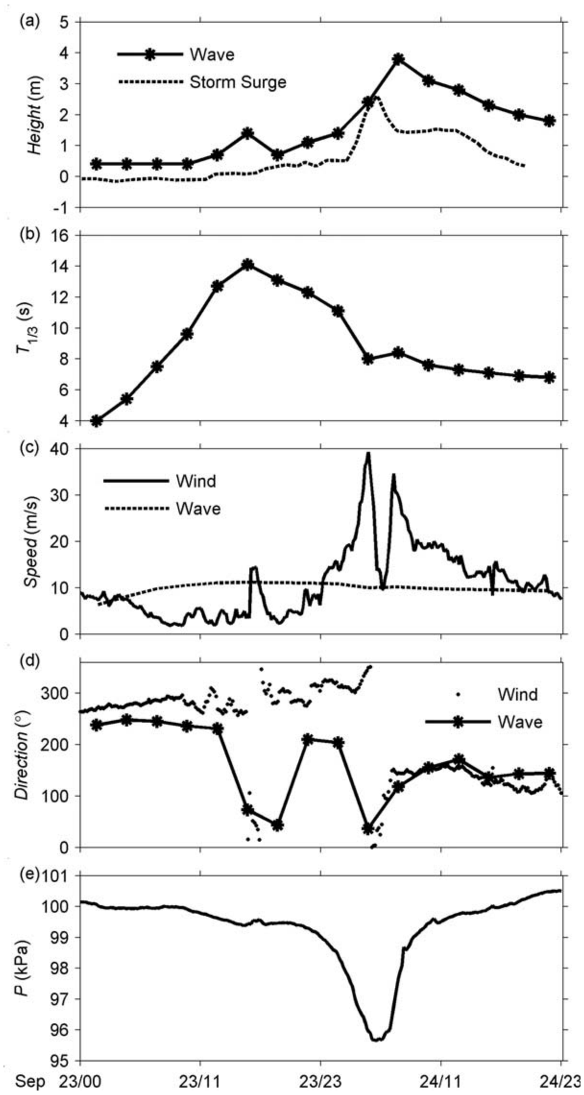

Figure 3. Time series during the passage of Typhoon Hagupit (23–24 September 2008). (a) Significant wave heights and water-level increases due to the storm surge (the storm surge data are extracted from the water-level measurements of a neighboring tide station [*Fu et al.*, 2009]), (b) significant wave period, and (c) wind speed at a height of 16.4 m and significant wave-phase speeds. The wave-phase speed corresponding to the significant wave period is calculated according to the explicit dispersion relationship given by *Fenton* [1988] with a water depth of 14 m. (d) The wind direction and wave direction and (e) the atmospheric pressure. The atmospheric quantities are 10 min means, and the oceanic quantities are 3 h means.

length z_o are determined by fitting the mean profile with equation (1) using the least squares method. The value of C_D at the 10 m reference height can be calculated via the following relationships:

$$C_D=\left(\frac{u_*}{U_{10}}\right)^2, \tag{2a}$$

$$C_D=\left(\frac{\kappa}{\ln\left(10/z_0\right)}\right)^2, \tag{2b}$$

where U_{10} is the Reynolds-averaged horizontal wind velocity at the reference height (10 m above the sea surface); the value is obtained by extrapolating the fitted logarithmic profile to 10 m. Clearly, one z_o corresponds to one unique C_D. Because the two variables provide the same information, we only analyze C_D.

3. Results and Discussion

3.1. Wave and Wind Conditions

The oceanic states and wind conditions prior to and during Typhoon Hagupit's approach are shown in Figure 3. The 10 min mean wind speed at a height of 16.4 m in Figure 3c ranges from 2.3 to 39.2 m s^{-1}. Prior to the arrival of the maximum wind, much of the wind data were between 2 and 9 m s^{-1}. Therefore, the COT was outside the direct influence of the typhoon during this period. Concurrently, the long swells already reached the observation site, and the mean of the significant wave period $T_{1/3}$ shown in Figure 3b was 8.9 s, with a peak at 14.1 s. These long swells appeared approximately 16 h before the arrival of the maximum wind speed, and the significant waves propagated at right angles to the local wind. The angle between the winds and the waves increased (Figure 3d). At 02:00 on 24 September, the crossing angle reached a maximum of 140°. With the arrival of the wind peaks, the crossing angle decreased sharply, and the wind and waves were nearly in the same direction (Figure 3d). The maximum significant wave height $H_{1/3}$ in Figure 3a increased to 3.8 m. With the decrease in the wind speed, the wave periods gradually decreased; however, nearly all the $T_{1/3}$ values exceeded 7 s. The influence of the storm surge was highly synchronized with the maximum wind, with a maximum water-level increment of 270 cm (Figure 3a).

Between the two peaks in the wind speed series in Figure 3c, a short calm period occurred. During this time, the local surface pressure was minimal at 956 hPa. According to these features and the position of the

COT relative to the typhoon track, we infer that the COT was within the eye of Typhoon Hagupit (i.e., an area of calm winds) between the two wind peaks.

Similarly to Hagupit, a mixture of swell and local wind-generated sea dominated the wave state prior to the approach of Typhoon Chanthu according to the wave period measurements. The 10 min mean wind speed at the 16.4 m height ranged from 2.3 to 33.7 m s^{-1}. After the arrival of the maximum wind, the wind directions persisted between 120° and 140°. The mean significant wave period and height were 8.6 s and 3.8 m, respectively. However, no reliable wave direction measurements were available during this typhoon. Uncertainties exist when analyzing the relative position of the COT in this typhoon. However, considering the characteristics of the wave height, the wave period, the wind direction and the COT's location relative to the typhoon track, we can infer the wave directions and the representativeness of the measurements during the typhoon.

For the calculations in sections 3.2 and 3.3, a mean for the significant wave period $T = 9.3$ s is obtained using the wave data corresponding to the wind data selected for the two typhoons.

As noted in section 1, the wave propagation directions are similar in the open ocean and at landfall in the vicinity of a hurricane [*Walsh et al.*, 2002]; thus, it is reasonable to follow the procedure used for the open ocean [*Black et al.*, 2007] to divide the storm wave state at landfall into three regions: (1) the rear sector, where the swell moves against the wind; (2) the right sector, where the swell travels with the wind; and (3) the left front sector, where the swell propagates across the wind. From the above illustrations, the analysis of the oceanic states, and the wind characteristics during Typhoons Hagupit and Chanthu, it is valid to assume that the low wind regime ($U_{10} < 15$ m s^{-1}) is in the outer edge of the typhoons, where the swell moves across the wind; the high wind regime corresponds to the right front sector, where the swell follows the wind and local wind-induced waves.

3.2. Friction Velocity and Drag Coefficient

The u_* deduced from the wind profiles recorded during Typhoons Hagupit and Chanthu are plotted in Figure 4a as a function of U_{10} from 2.7 to 41.9 m s^{-1}. The friction velocity approximately increases with U_{10} from 2.7 to 29.3 m s^{-1}. Beyond this range, a saturation or slight decrease in u_* is observed, although the data for high winds are sparse and large uncertainties may exist. Because a data gap of 2 m s^{-1} exists between the wind speeds of 29.7 and 31.7 m s^{-1}, u_* is assumed to reach its maximum value at approximately 30 m s^{-1}. The u_* deduced from the 10 min mean wind speed is shown. The data point clusters of the two types of u_* overlap, and no significant difference exists between the two results.

Based on the U_{10} and C_D data reported in the literature [*Black et al.*, 2007; *Edson et al.*, 2007; *Holthuijsen et al.*, 2012; *Jarosz et al.*, 2007; *Large and Pond*, 1981; *Wu*, 1982], the corresponding u_* values are deduced ($u_* = C_D^{1/2} U_{10}$). Our data are in good agreement with the calculated u_* values up to approximately 10 m s^{-1}. Beyond this wind speed, our u_* values gradually and significantly exceed the calculated values up to wind speeds of 29.3 m s^{-1}. For higher wind speeds, the few cited u_* values [*Holthuijsen et al.*, 2012; *Jarosz et al.*, 2007; *Powell et al.*, 2003] somewhat coincide with our u_* values within the range of 1.2–1.9 m s^{-1}, and the predictions of the unbounded linear C_D formulation [*Wu*, 1982] appear as outliers. *Powell et al.* [2003] reported that u_* increases with U_{10} up to 40 m s^{-1} and then levels off. The u_* values reported by *Jarosz et al.* [2007] and *Holthuijsen et al.* [2012] are also shown to level off or slightly decrease after reaching maximum values (as shown in Figure 4a). The critical wind speeds deduced from the two papers are also approximately 40 m s^{-1}; however, large uncertainties exist in our results and in the previous results; thus, whether u_* levels off or decreases under extreme wind speeds remains elusive. The behavior of u_* at extreme wind speeds is very similar to that of scatterometer measurements of normalized radar cross sections [*Donnelly et al.*, 1999; *Hersbach et al.*, 2007], which were found to reach saturation at wind speeds exceeding 25 m s^{-1}. Surface roughness dominates the microwave emissions from the ocean [*Wentz*, 1992]; the saturation of normalized radar cross sections with increasing U_{10} values is thus associated with the saturation of the surface roughness and surface stress.

The comparison and analysis above shows that the measured u_* values over coastal shallow waters have common and unique features relative to the published values over the deep open ocean, i.e., a good agreement in low winds $U_{10} \le 10$ m s^{-1}, which gradually and significantly increase (10 m s$^{-1} < U_{10} \le 30$ m s^{-1}) and then coincide again when 30 m s$^{-1} < U_{10} \le \sim$40 m s^{-1}. However, the critical wind speeds at which u_*

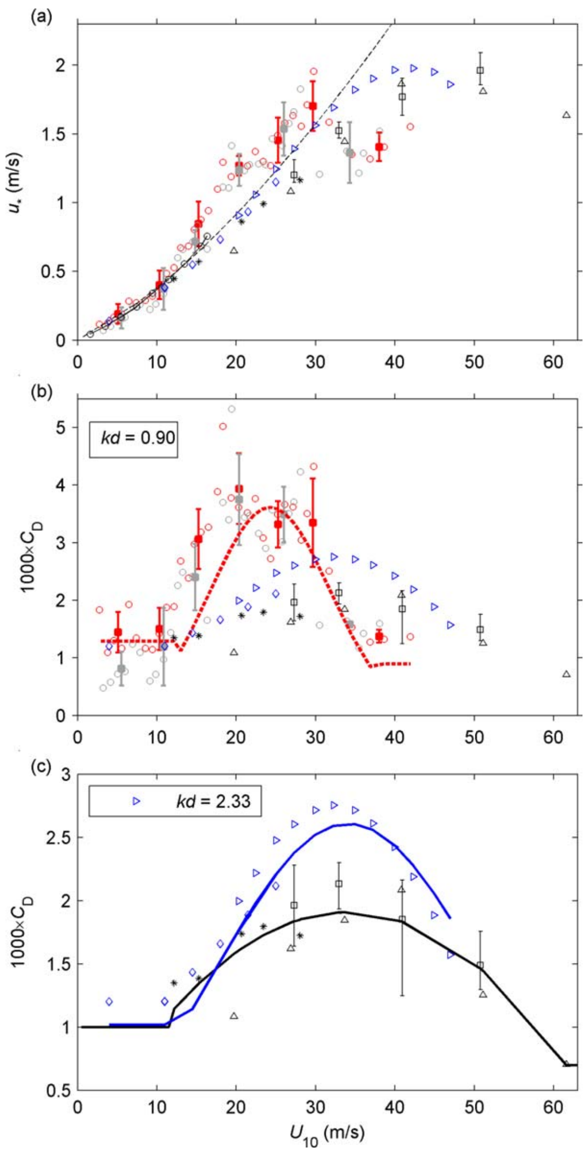

Figure 4. (a) Dependence of friction velocity u_* and (b) drag coefficient C_D over various water depths over the continental shelf and (c) in the open ocean on the 10 m wind speed U_{10}. The red open circles are the assessed values in each 1 m s^{-1} wind speed bin according to the lowest level wind speed; the red squares and vertical bars represent the means and 2 times the standard deviations in each 5 m s^{-1} of U_{10}, respectively. The corresponding gray open circles, squares, and vertical bars are the results from the 10 min mean wind data. In Figure 6b, the red-dashed line is produced by equation (4) with a water depth $d = 14$ m. Chronologically, the cited C_D and u_* (deduced from their C_D and U_{10} relationships, except for the case of *Powell et al.* [2003], where u_* was directly given) results are shown: *Large and Pond* [1981] for $d = 59$ m (blue diamonds), *Wu* [1982] (black dashed line), *Powell et al.* [2003] for the open ocean (black squares with bars), *Edson et al.* [2007] for $d = 15$ m (black solid line with open circles), *Black et al.* [2007] for the open ocean (black stars), *Jarosz et al.* [2007] for $d = 69$–89 m (right-pointing blue triangles), and *Holthuijsen et al.* [2012] for the open ocean (upward-pointing black triangles). Specifically, the symbols for *Powell et al.* [2003] are their results from the 10 to 150 m layer, the symbols for *Jarosz et al.* [2007] are for a resistance coefficient of r = 0.0505 cm s^{-1}, and the symbols for *Holthuijsen et al.* [2012] are from their Figure 6a. In Figure 6c, the blue solid line is produced by equation (4) for $d = 89$ m; the black solid line is produced by equation (4) by assuming $d = 10{,}000$ m.

reaches its maximum value and then levels off is significantly less than those speeds over deeper water [*Holthuijsen et al.*, 2012; *Jarosz et al.*, 2007; *Powell et al.*, 2003].

The dependency of C_D on the wind speed U_{10} is shown in Figure 4b. For $U_{10} \leq 10$ m s^{-1}, the range of our C_D values covers the variation in the reported values. An apparent discrepancy exists between our C_D and the cited values starting at approximately 10 m s^{-1}. Between 14 and $\sim$30 m s^{-1}, our C_D values have almost no overlap with the cited values. After reaching its maximum and $U_{10} > \sim$30 m s^{-1}, C_D significantly decreases. For $U_{10} \approx$ 40 m s^{-1}, C_D reaches 1.3 $\times$ 10^{-3}. The open ocean results [*Holthuijsen et al.*, 2012] also reported a significant decrease in C_D, a very low limiting value (0.7 $\times$ 10^{-3}) as U_{10} increases to approximately 60 m s^{-1}, and a coincidence of foam streaks and droplets at the surface.

Figure 4b also shows the C_D values from the 10 min wind speed. Note that an evident difference exists between the two results for $U_{10} \leq 10$ m s^{-1}, and the bin mean of the 1 min results exceeds that of the 10 min results by 75%. For U_{10} greater than 10 m s^{-1}, the data point clusters of the two results overlap and no significant differences exist.

In Figure 4b, another remarkable feature is noted: in high winds, the C_D curves demonstrate a systematic shift from the lower-right to the upper-left in the U_{10}-C_D frame of reference. The shifts occur in the following order: *Holthuijsen et al.* [2012], *Powell et al.* [2003], *Jarosz et al.* [2007], and the present study. The shift of the C_D curves implies a change in the critical wind speed at which point the drag coefficient reaches its maximum value (denoted by U_{10c} hereafter). The U_{10c} from different studies and the corresponding water depths/laboratory conditions are listed in Table 1. Depending on the selected bin width of the wind speed, some studies may obtain large uncertainties when determining U_{10c}. For example, *Holthuijsen et al*. [2012] selected a 10 m s^{-1} wind speed bin width; thus, larger uncertainty may exist in their U_{10c}. Despite these uncertainties, the trend in which U_{10c} shifts toward low values as the water depth becomes shallower is evident in Figure 4b. Therefore, we postulate from the analysis that the water depth change will change the wind-speed dependence of C_D, and it can be considered an important modulation factor for the dependence of C_D on U_{10}.

To account for the above-described effect of water depth on the behavior of C_D, we consider the following aspects. First, previous measurements [e.g., *Gao et al*., 2009; *Geernaert et al*., 1986; *Oost et al*., 2001] have shown that the C_D over shallow water is higher than that over deep water at the same wind speed and have related this phenomenon to wave state parameters, e.g., wave age. Here, we also attribute the variation in C_D to the change in the wave state from the perspective of the effect of water depth on the wave state. A significant wave is chosen as the representative wave state parameter. More details are provided in section 3.3. Second, strong wave breaking at high winds and the presence of sea spray associated with wave breaking are often invoked to explain the leveling off or decrease in C_D with wind speed [e.g., *Bye and Wolff*, 2008; *Powell et al*., 2003; *Shtemler et al*., 2010; *Soloviev and Lukas*, 2010]. Therefore, the variable dependency of C_D on wind speeds with different water depths may be a manifestation of the water depth modulating the process of wave breaking. To illustrate this point, we adopt the global wave steepness [*Wu and Nepf*, 2002] S (defined as the criterion for wave breaking). Although wave breaking is often perceived as a random process [*Babanin*, 2009], without the loss of generality, S enables us to make preliminary quantitative assessments. In shallow water, in addition to the wind-induced wave growth, the effect of shoaling increases the wave amplitude and steepness; thus, wave breaking in high winds is the combination of white-capping and depth-induced wave breaking. Consequently, the wind speed values at which waves start to break in shallow water (our study) can be smaller than those over deep open water. Here, the shoaling coefficient K_{sh} [*Holthuijsen*, 2007, p. 201] is adopted to calculate the dependence of S on water depth. For the swell with a wave period of $T = 9.3$ s described in section 3.1, the ratio of the steepness in water depth $d = 14$ m to that in deep water S/S_∞ is 1.30. Because there is no exact water depth information from the studies of *Powell et al*. [2003] and *Holthuijsen et al*. [2012], we estimated the ratio between our wave steepness to the theoretical value S_∞ obtained from above: $S/S_\infty = 1.3$. According to the water depth information supplied by Ewa Jarosz (69–89 m; personal communication, 2013), the ratio of our result to that reported by *Jarosz et al*. [2007] is also 1.30. According to Table 1, the ratios of the U_{10c} reported by *Holthuijsen et al*. [2012], *Powell et al*. [2003], *Jarosz et al*. [2007], and the present study are 40, 34, 30, and 24 m s^{-1}, respectively, and the ratios of the first three U_{10c} values to our U_{10c} value are 1.67, 1.42, and 1.25, respectively. Accounting for the large uncertainties in both U_{10c} [*Holthuijsen et al*., 2012; *Powell et al*., 2003] and the breaking criteria, it may be reasonable to speculate that the change in U_{10c} is associated with the depth-induced wave-steepness increase. We are not suggesting that the water depth is the only contributing factor to C_D, which is a function of U_{10}. Rather, this study provides evidence that the air-sea momentum exchange at high wind speeds might be affected by the water depth through depth-induced changes in wave steepness. Further details are provided in the following paragraphs to formulate a water-depth-dependent parameterization for C_D.

3.3. A C_D Parameterization Dependent on Water Depth and Wind Speed

The wind stress over the ocean is dependent on wave states. Numerous studies have focused on the air-sea drag from this perspective, and many formulas have been proposed based on wave parameters. A dimensional analysis yields the following:

$$C_D = C_D\left(\frac{U_{10}}{(gz_1)^{1/2}}, \frac{gd}{U_{10}^2}, \frac{U_{10}}{c}, S\right), \tag{3}$$

where z_1 is a reference height above the sea surface (often 10 m), g is the gravitational acceleration, and c is the wave speed. However, simultaneous measurements of wave age and wave steepness in hurricane/typhoon-generating seas are not available. The studies on wave spectra in hurricane-generating seas [*Ochi*, 2003] show that the wave energy is highly concentrated around a modal frequency. At the growing stage of the wave spectra, the increasing rate of the wave energy near the modal frequency is much greater than that at any other frequency in the spectrum. Studies have shown that remotely generated swells dominate

10.1002/2014JC010283

nearly all quadrants of a hurricane [*Black et al*., 2007; *Walsh et al*., 2002; *Wright et al*., 2001; *Young*, 2006] in both the open ocean and the shallow coastal water at landfall. These measurements may indicate that it is appropriate to select significant or dominant waves when modeling hurricane-induced sea states under the assumption of infinite wind fetch and duration. With unlimited wind fetch and duration, the significant wave height and period in deep water depend only on the local wind speed [e.g., *Holthuijsen*, 2007]. When the water depth decreases and affects the waves, the significant wave height and period depend on both the local wind speed and water depth, i.e., SMB relations (Sverdrup, Munk, and Bretschneider) [see *Holthuijsen*, 2007].

In reality, the results in Figure 4b imply that C_D depends on both the water depth and wind speeds simultaneously. The results of *Large and Pond* [1981] ($d = 59$ m) and *Jarosz et al*. [2007] ($d = 69$–89 m) are similar for intermediate depths within their common wind speed range. Similarly, the results of *Black et al*. [2007] and *Powell et al*. [2003], both of which are based on open-ocean measurements, also tend to coincide in their common wind speed range. Here, we attempt to fit a C_D formula as a function of both water depth and wind speed by following several steps based on the sparse data on high winds. First, a parabola is fitted according to the data from the open-ocean results [*Black et al*., 2007; *Holthuijsen et al*., 2012; *Powell et al*., 2003]:

$$1000 \times C_D = -1.85\tilde{u}^2 + 3.70\tilde{u} - 0.05, \tag{4}$$

where $\tilde{u} = U_{10}/U_{ref}$. Note that U_{ref} corresponds to the wind speed at which C_D is maximized and $U_{ref} = U_{10c\infty} = 34$ m s^{-1} is the critical wind speed over an infinite water depth. Considering the differences in U_{10c} at the different water depths noted above, we introduce the ratios of global wave steepness at different water depths relative to that at an infinite water depth to determine the change in U_{ref} with water depth:

$$r_{slope} = \frac{ka}{k_\infty a_\infty} = \frac{k}{k_\infty} \times \sqrt{\frac{c_{g\infty}}{c_g}}, \tag{5}$$

where k is the wave number and a is the wave amplitude. The ratio is based on the conversion of wave energy. Thus, the definition of U_{ref} is as follows:

$$U_{ref} = \frac{U_{10c\infty}}{r_{slope}}. \tag{6}$$

Second, the hyperbolic tangent function, which is widely utilized in the description of dependencies of significant wave heights and periods on water depth and wind speed [*Holthuijsen*, 2007, pp. 247–248, and references therein], is introduced into the formula to establish the dependence of the C_D magnitude on the water depth. However, with only the combination of a parabola and a hyperbolic tangent function, the formula and the existing data cannot be well fitted. Thus, an exponential function is also introduced to modify the amplitude of the fitted function. Finally, a C_D formula, which depends on both wind speed and water depth, is acquired:

$$1000 \times C_D = \max\left\{ \frac{\hbar}{b + \tanh\left(\frac{gd}{u_{c\infty}^2}\right)^b},\ \frac{\exp\left[-\frac{(U_{10}-u_{ref})^2}{gd}\right]}{\tanh\left(\frac{gd}{u_{c\infty}^2}\right)^b}\left(p(1)\tilde{u}^2 + p(2)\tilde{u} + p(3)\right) \right\}, \tag{7}$$

where the first term corresponds to the performance of C_D in very low and high wind speeds and $\hbar$ is the low threshold of the C_D values in low and high winds over an infinite water depth. In low winds ($U_{10} < u_{ref}$), $\hbar$ is set to 1. In high winds, $\hbar$ is set to 0.65. b is fitted as 0.25.

As shown in Figure 4c, the results from *Jarosz et al*. [2007], which are based on intermediate water depths, strongly agree with the prediction of this formula. If we consider the scattered data shown in Figure 4b, then our results also agree with the formula.

Equation (7) is tested in the simulations of Typhoon Nanmadol (2011) with the Global/Regional Assimilation and Prediction System (GRAPES) model [*Chen et al*., 2008] with a grid resolution 0.09°. The initial field is supplied by the NCEP 0.5° × 0.5° analysis field. The C_D in the operational GRAPES is deduced from a modified Charnock relationship [*Smith*, 1988], and it increases monotonically with wind speed up to 35 m s^{-1} and then levels off. The relationship is expressed as follows:

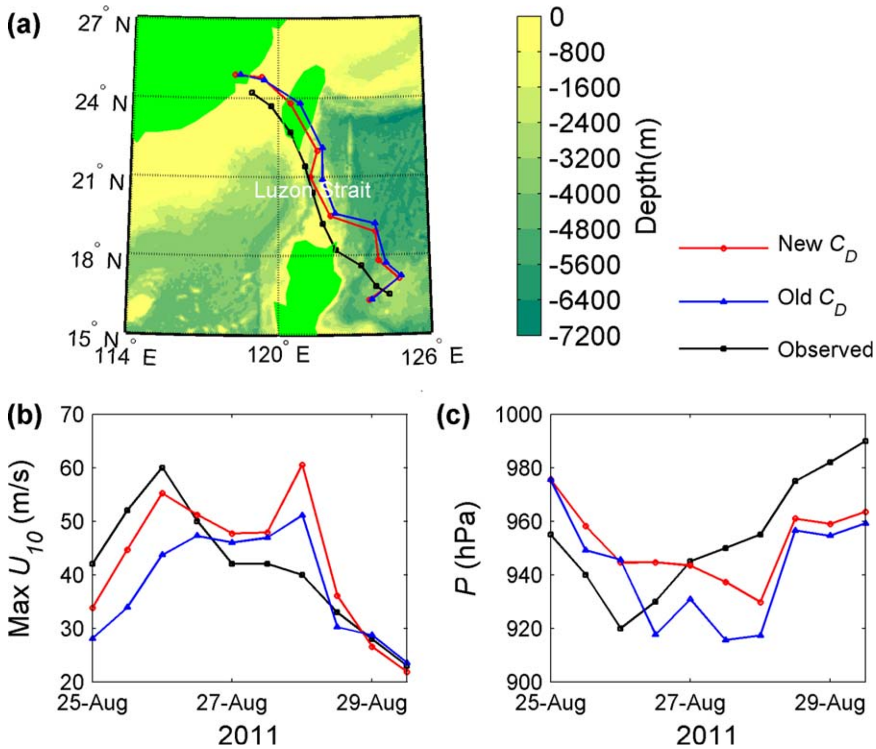

Figure 5. (a) Track, (b) maximum 10 m wind speed, and (c) central pressure of Typhoon Nanmadol (2011). The three subgraphs share the same legend: the predictions with the new C_D parameterization in equation (4) are denoted by red lines with circles, the predictions with the C_D formula in equation (5) are shown as blue lines with triangles, and the observations from the China Meteorological Administration are shown as black lines with squares.

$$1000\times z_0=\begin{cases}15.6\dfrac{u_*^2}{g}+10^{-2} & U_{10}<35ms^{-1}\\ 2.82 & U_{10}\geq 35ms^{-1}\end{cases}. \tag{8}$$

The +48 h predictions of the track, maximum 10 m wind speed and central pressure are shown in Figure 5. The track is based on the 850 hPa geopotential heights. As shown in Figure 5a, with the new parameterization, the simulated track is improved, particularly in the Luzon Strait, where the terrain resolution is relatively high. On average, the absolute track error is reduced by 7.6 km relative to the operational error. The maximum U_{10} and central pressure with the new C_D parameterization are more similar to the observations than to the operational results; the absolute errors of the maximum U_{10} and central pressure are reduced by 1.6 m s^{-1} and 4.9 hPa, on average, respectively. However, the intensity of Nanmadol on 28 August using both of the C_D parameterizations is not consistent with the actual conditions.

4. Conclusions

Based on the observations from a coastal tower in the South China Sea during typhoon passages, this work investigates the air-sea momentum exchange at extreme wind speeds over shallow waters. In contrast to many studies on high winds over the open ocean, we were able to obtain data over the nearshore water, which are potentially pertinent to studies on hurricane landfalls. By comparing our nearshore observational results with the results of previous studies over deeper waters at high wind speeds, we confirm that the dependence of C_D on wind speed is modified by water depth. For example, relative to the results from the deep open ocean [e.g., *Black et al.*, 2007; *Holthuijsen et al.*, 2012; *Powell et al.*, 2003] and intermediate water depths [e.g., *Jarosz et al.*, 2007; *Large and Pond*, 1981], the critical wind speed at which C_D is maximized decreases by approximately 5–15 m s^{-1}. The shoaling effect, combined with the wave conditions during a typhoon/hurricane, is invoked to explain the above findings quantitatively. Furthermore, we calculate C_D as a function of both wind speed and water depth. Numerical tests show that the predictions are consistent with the observations; the absolute errors of the +48 h prediction of the typhoon track, the maximum 10 m wind speed and the central pressure are reduced by 7.6 km, 1.6 m s^{-1}, and 4.9 hPa, on average, respectively, compared with an operational C_D parameterization that assumes that C_D levels off during high winds.

The findings of this study may also have implications for coastal wave and sea spray models. The C_D schemes of *Wu* [1982] and the recently modified version [*Zijlema et al*., 2012] used in the coastal wave model SWAN [*Booij et al*., 1999] provide results that are dramatically different from our results. The use of our C_D scheme may avoid the underprediction of wave growth rates [*Peirson and Garcia*, 2008] in coastal waters. In sea spray models [*Bao et al*., 2011], the critical wind speed at which the microphysics of the spray changes is not clear, and a value of approximately 30 m s^{-1} is somewhat arbitrarily chosen. However, our results imply that the critical wind speed may not be constant, and it should change with the water depth.

As previous studies have extensively noted, the air-sea momentum flux is not only a function of wind speed; it also depends on the wave state [*Guan and Xie*, 2004; *Smith et al*., 1992; *Toba et al*., 1990]. We account for the effects of the sea state according to the fully developed significant waves in typhoon/hurricane scenarios. Studies have shown that an asymmetric distribution of C_D induced by different sea states may play a significant role in determining the wind structure within the typhoon and may affect typhoon/hurricane forecasts. Future work will include exploring the dependence of C_D on sea states in different sectors of typhoon/hurricanes to advance our understanding of the air-sea momentum exchange under extreme wind conditions.

Acknowledgments
The authors appreciate the support from the Ministry of Science and Technology of China (2009CB421500), the National Natural Science Foundation of China (41205011, 41075051, and 40830959), the Special Funds for the Science and Technology of China (GYHY201106036), and the Guangdong Science and Technology Plan Project (2012A061400012). The authors also appreciate the observations provided by the Guangzhou Institute of Tropical and Marine Meteorology, China Meteorology Administration (CMA). The data in the figures and tables can be acquired by contacting the author via email: zhaozk@grmc.gov.cn.

References

Alamaro, M., K. Emanuel, J. Colton, W. McGillis, and J. B. Edson (2002), Experimental investigation of air-sea transfer of momentum and enthalphy at high wind speed, paper presented at 25th Conference on Hurricanes and Tropical Meteorolgy, Am. Meteorol. Soc., San Diego, Calif.
Anctil, F., and M. A. Donelan (1996), Air-water momentum flux observations over shoaling waves, *J. Phys. Oceanogr.*, *26*(7), 1344–1353.
Andreas, E. L. (2004), Spray stress revisited, *J. Phys. Oceanogr.*, *34*(6), 1429–1440, doi:10.1175/1520-0485(2004)034<1429:SSR>2.0.CO;2.
Babanin, A. (2009), Breaking of ocean surface waves, *Acta Phys. Slovaca*, *59*(4), 305–535, doi:10.2478/v10155-010-0097-5.
Bao, J. W., C. W. Fairall, S. A. Michelson, and L. Bianco (2011), Parameterizations of sea-spray impact on the air-sea momentum and heat fluxes, *Mon. Weather Rev.*, *139*(12), 3781–3797, doi:10.1175/MWR-D-11-00007.1.
Bell, M. M., M. T. Montgomery, and K. A. Emanuel (2012), Air-sea enthalpy and momentum exchange at major hurricane wind speeds observed during CBLAST, *J. Atmos. Sci.*, *69*(11), 3197–3222, doi:10.1175/JAS-D-11-0276.1.
Black, P. G., E. A. D'Asaro, T. B. Sanford, W. M. Drennan, J. A. Zhang, J. R. French, P. P. Niiler, E. J. Terrill, and E. J. Walsh (2007), Air-sea exchange in hurricanes: Synthesis of observations from the coupled boundary layer air-sea transfer experiment, *Bull. Am. Meteorol. Soc.*, *88*(3), 357–374, doi:10.1175/BAMS-88-3-357.
Booij, N., R. C. Ris, and L. H. Holthuijsen (1999), A third-generation wave model for coastal regions. 1: Model description and validation, *J. Geophys. Res.*, *104*(C4), 7649–7666, doi:10.1029/98JC02622.
Bye, J., and J.-O. Wolff (2008), Charnock dynamics: A model for the velocity structure in the wave boundary layer of the air-sea interface, *Ocean Dyn.*, *58*(1), 31–42.
Charnock, H. (1955), Wind stress on a water surface, *Q. J. R. Meteorol. Soc.*, *81*(350), 639–640, doi:10.1002/qj.49708135027.
Chen, D., J. Xue, X. Yang, H. Zhang, X. Shen, J. Hu, Y. Wang, L. Ji, and J. Chen (2008), New generation of multi-scale NWP system (GRAPES): General scientific design, *Chin. Sci. Bull.*, *53*(22), 3433–3445, doi:10.1007/s11434-008-0494-z.
Donelan, M. A., B. K. Haus, N. Reul, W. J. Plant, M. Stiassnie, H. C. Graber, O. B. Brown, and E. S. Saltzman (2004), On the limiting aerodynamic roughness of the ocean in very strong winds, *Geophys. Res. Lett.*, *31*, L18306, doi:10.1029/2004GL019460.
Donelan, M. A., M. Curcic, S. S. Chen, and A. K. Magnusson (2012), Modeling waves and wind stress, *J. Geophys. Res.*, *117*, C00J23, doi:10.1029/2011JC007787.
Donnelly, W. J., J. R. Carswell, R. E. McIntosh, P. S. Chang, J. Wilkerson, F. Marks, and P. G. Black (1999), Revised ocean backscatter models at C and Ku band under high-wind conditions, *J. Geophys. Res.*, *104*(C5), 11,485–11,497, doi:10.1029/1998JC900030.
Edson, J., et al. (2007), The coupled boundary layers and air-sea transfer experiment in low winds, *Bull. Am. Meteorol. Soc.*, *88*(3), 341–356, doi:10.1175/BAMS-88-3-341.
Fenton, J. D. (1988), The numerical solution of steady water wave problems, *Comput. Geosci.*, *14*(3), 357–368, doi:10.1016/0098-3004(88)90066-0.
Fu, X., J. Dong, J. Ma, T. Zhang, and F. Yu (2009), Analysis and numerical simulation of the storm surge caused by Typhoon 'Hagupit' [in Chinese], *Mar. Forecasts*, *26*(4), 68–75.
Gao, Z., Q. Wang, and M. Zhou (2009), Wave-dependence of friction velocity, roughness length, and drag coefficient over coastal and open water surfaces by using three databases, *Adv. Atmos. Sci.*, *26*(5), 887–894.
Garratt, J. R. (1977), Review of drag coefficients over oceans and continents, *Mon. Weather Rev.*, *105*(7), 915–929, doi:10.1175/1520-0493(1977)105<0915:RODCOO>2.0.CO;2.
Geernaert, G. L., K. B. Katsaros, and K. Richter (1986), Variation of the drag coefficient and its dependence on sea state, *J. Geophys. Res.*, *91*(C6), 7667–7679, doi:10.1029/JC091iC06p07667.
Gopalakrishnan, S., Q. Liu, T. Marchok, D. Sheinin, N. Surgi, M. Tong, V. Tallapragada, R. Tuleya, R. Yablonsky, and X. Zhang (2011), Hurricane weather research and forecasting (HWRF) model: 2011 scientific documentation, 82 pp., Dev. Testbed Cent., Boulder, Colo.
Grachev, A. A., and C. W. Fairall (2001), Upward momentum transfer in the marine boundary layer, *J. Phys. Oceanogr.*, *31*(7), 1698–1711, doi:10.1175/1520-0485(2001)031<1698:UMTITM>2.0.CO;2.
Guan, C., and L. Xie (2004), On the linear parameterization of drag coefficient over sea surface, *J. Phys. Oceanogr.*, *34*(12), 2847–2851, doi:10.1175/JPO2664.1.
Hersbach, H., A. Stoffelen, and S. de Haan (2007), An improved C-band scatterometer ocean geophysical model function: CMOD5, *J. Geophys. Res.*, *112*, C03006, doi:10.1029/2006JC003743.

Holthuijsen, L. H. (2007), *Waves in Oceanic and Coastal Waters*, Cambridge Univ. Press, Cambridge, U. K.

Holthuijsen, L. H., M. D. Powell, and J. D. Pietrzak (2012), Wind and waves in extreme hurricanes, *J. Geophys. Res.*, *117*, C09003, doi:10.1029/2012JC007983.

Jarosz, E., D. A. Mitchell, D. W. Wang, and W. J. Teague (2007), Bottom-up determination of air-sea momentum exchange under a major tropical cyclone, *Science*, *315*(5819), 1707–1709, doi:10.1126/science.1136466.

Large, W. G., and S. Pond (1981), Open ocean momentum flux measurements in moderate to strong winds, *J. Phys. Oceanogr.*, *11*(3), 324–336.

Liu, B., C. Guan, and L. Xie (2012), The wave state and sea spray related parameterization of wind stress applicable from low to extreme winds, *J. Geophys. Res.*, *117*, C00J22, doi:10.1029/2011JC007786.

Makin, V. K., and V. N. Kudryavtsev (2002), Impact Of dominant waves on sea drag, *Boundary Layer Meteorol.*, *103*(1), 83–99, doi:10.1023/A:1014591222717.

Montgomery, M. T., R. K. Smith, and S. V. Nguyen (2010), Sensitivity of tropical-cyclone models to the surface drag coefficient, *Q. J. R. Meteorol. Soc.*, *136*(653), 1945–1953, doi:10.1002/qj.702.

Moon, I.-J., I. Ginis, and T. Hara (2004), Effect of surface waves on air-sea momentum exchange. Part II: Behavior of drag coefficient under tropical cyclones, *J. Atmos. Sci.*, *61*(19), 2334–2348, doi:10.1175/1520-0469(2004)061<2334:EOSWOA>2.0.CO;2.

Moon, I.-J., I. Ginis, T. Hara, and B. Thomas (2007), A physics-based parameterization of air-sea momentum flux at high wind speeds and its impact on hurricane intensity predictions, *Mon. Weather Rev.*, *135*(8), 2869–2878, doi:10.1175/MWR3432.1.

Moon, I.-J., I. Ginis, and T. Hara (2008), Impact of the reduced drag coefficient on ocean wave modeling under hurricane conditions, *Mon. Weather Rev.*, *136*(3), 1217–1223, doi:10.1175/2007MWR2131.1.

Mueller, J., and F. Veron (2009), Nonlinear formulation of the bulk surface stress over breaking waves: Feedback mechanisms from air-flow separation, *Boundary Layer Meteorol.*, *130*(1), 117–134, doi:10.1007/s10546-008-9334-6.

Ochi, M. K. (2003), *Hurricane-Generated Seas*, 155 pp., Elsevier, Oxford, U. K.

Oost, W. A., G. J. Komen, C. M. J. Jacobs, C. van Oort, and H. Bonekamp (2001), Indications for a wave dependent charnock parameter from measurements during ASGAMAGE, *Geophys. Res. Lett.*, *28*(14), 2795–2797, doi:10.1029/2001GL013035.

Peirson, W. L., and A. W. Garcia (2008), On the wind-induced growth of slow water waves of finite steepness, *J. Fluid Mech.*, *608*, 243–274, doi:10.1017/s002211200800205x.

Powell, M. D., P. J. Vickery, and T. A. Reinhold (2003), Reduced drag coefficient for high wind speeds in tropical cyclones, *Nature*, *422*(6929), 279–283, doi:10.1038/nature01481.

Shtemler, Y. M., E. Golbraikh, and M. Mond (2010), Wind-wave stabilization by a foam layer between the atmosphere and the ocean, *Dyn. Atmos. Oceans*, *50*(1), 1–15, doi:10.1016/j.dynatmoce.2009.08.002.

Smith, S. D. (1988), Coefficients for sea surface wind stress, heat flux, and wind profiles as a function of wind speed and temperature, *J. Geophys. Res.*, *93*(C12), 15,467–15,472, doi:10.1029/JC093iC12p15467.

Smith, S. D., et al. (1992), Sea surface wind stress and drag coefficients: The HEXOS results, *Boundary Layer Meteorol.*, *60*(1), 109–142, doi:10.1007/BF00122064.

Soloviev, A., and R. Lukas (2010), Effects of bubbles and sea spray on air–sea exchange in hurricane conditions, *Boundary Layer Meteorol.*, *136*(3), 365–376, doi:10.1007/s10546-010-9505-0.

Stull, R. B. (1988), *An Introduction to Boundary Layer Meteorology*, Kluwer Acad. Publ., Dordrecht, Netherlands.

Takagaki, N., S. Komori, N. Suzuki, K. Iwano, T. Kuramoto, S. Shimada, R. Kurose, and K. Takahashi (2012), Strong correlation between the drag coefficient and the shape of the wind sea spectrum over a broad range of wind speeds, *Geophys. Res. Lett.*, *39*, L23604, doi:10.1029/2012GL053988.

Toba, Y., N. Iida, H. Kawamura, N. Ebuchi, and I. S. F. Jones (1990), Wave dependence of sea-surface wind stress, *J. Phys. Oceanogr.*, *20*(5), 705–721, doi:10.1175/1520-0485(1990)020<0705:WDOSSW>2.0.CO;2.

Toffoli, A., L. Loffredo, P. Le Roy, J. M. Lefèvre, and A. V. Babanin (2012), On the variability of sea drag in finite water depth, *J. Geophys. Res.*, *117*, C00J25, doi:10.1029/2011JC007857.

Troitskaya, Y. I., D. A. Sergeev, A. A. Kandaurov, G. A. Baidakov, M. A. Vdovin, and V. I. Kazakov (2012), Laboratory and theoretical modeling of air-sea momentum transfer under severe wind conditions, *J. Geophys. Res.*, *117*, C00J21, doi:10.1029/2011JC007778.

Walsh, E. J., C. W. Wright, D. Vandemark, W. B. Krabill, A. W. Garcia, S. H. Houston, S. T. Murillo, M. D. Powell, P. G. Black, and F. D. Marks (2002), Hurricane directional wave spectrum spatial variation at landfall, *J. Phys. Oceanogr.*, *32*(6), 1667–1684, doi:10.1175/1520-0485(2002)032<1667:HDWSSV>2.0.CO;2.

Walsh, K. J. E., P. Sandery, G. B. Brassington, M. Entel, C. Siegenthaler-LeDrian, J. D. Kepert, and R. Darbyshire (2010), Constraints on drag and exchange coefficients at extreme wind speeds, *J. Geophys. Res.*, *115*, C09007, doi:10.1029/2009JC005876.

Wentz, F. J. (1992), Measurement of oceanic wind vector using satellite microwave radiometers, *IEEE Trans. Geosci. Remote Sens.*, *30*(5), 960–972, doi:10.1109/36.175331.

Wright, C. W., E. J. Walsh, D. Vandemark, W. B. Krabill, A. W. Garcia, S. H. Houston, M. D. Powell, P. G. Black, and F. D. Marks (2001), Hurricane directional wave spectrum spatial variation in the open ocean, *J. Phys. Oceanogr.*, *31*(8), 2472–2488, doi:10.1175/1520-0485(2001)031<2472:HDWSSV>2.0.CO;2.

Wu, C. H., and H. M. Nepf (2002), Breaking criteria and energy losses for three-dimensional wave breaking, *J. Geophys. Res.*, *107*(C10), 3177, doi:10.1029/2001JC001077.

Wu, J. (1982), Wind-stress coefficients over sea surface from breeze to hurricane, *J. Geophys. Res.*, *87*(C12), 9704–9706, doi:10.1029/JC087iC12p09704.

Yelland, M., and P. K. Taylor (1996), Wind stress measurements from the open ocean, *J. Phys. Oceanogr.*, *26*(4), 541–558, doi:10.1175/1520-0485(1996)026<0541:WSMFTO>2.0.CO;2.

Young, I. R. (2006), Directional spectra of hurricane wind waves, *J. Geophys. Res.*, *111*, C08020, doi:10.1029/2006JC003540.

Zedler, S. E., P. P. Niiler, D. Stammer, E. Terrill, and J. Morzel (2009), Ocean's response to Hurricane Frances and its implications for drag coefficient parameterization at high wind speeds, *J. Geophys. Res.*, *114*, C04016, doi:10.1029/2008JC005205.

Zhang, J., W. Feng, G. Li, and W. Xu (2011), Analysis and numerical simulation of the storm surge caused by the typhoon 'Chanthu' [in Chinese], *Mar. Sci. Bull.*, *30*(4), 367–370.

Zhao, Z., J. Liang, Q. Wan, Y. Qi, F. Liao, M. Y. Zhou, C. Liu, J. Huang, H. Huang, and W. Mao (2011), Observational analysis of air-sea momentum exchange in strong wind condition [in Chinese], *J. Trop. Meteorol.*, *27*(6), 899–904.

Zijlema, M., G. P. van Vledder, and L. H. Holthuijsen (2012), Bottom friction and wind drag for wave models, *Coastal Eng.*, *65*, 19–26, doi:10.1016/j.coastaleng.2012.03.002.

Zweers, N. C., V. K. Makin, J. W. de Vries, and G. Burgers (2010), A sea drag relation for hurricane wind speeds, *Geophys. Res. Lett.*, *37*, L21811, doi:10.1029/2010GL045002.